

Entanglement Distribution in Satellite-based Dynamic Quantum Networks

Alena Chang, *Student Member, IEEE*, Yinxin Wan, *Student Member, IEEE*, Guoliang Xue, *Fellow, IEEE*, Arunabha Sen, *Senior Member, IEEE*

Abstract—Low Earth Orbit (LEO) satellites present a compelling opportunity for the establishment of a global quantum information network. However, satellite-based entanglement distribution from a networking perspective has not been fully investigated. Existing works often do not account for satellite movement over time when distributing entanglement and/or often do not permit entanglement distribution along inter-satellite links, which are two shortcomings we address in this paper. We first define a system model which considers both satellite movement over time and inter-satellite links. We next formulate the optimal entanglement distribution (OED) problem under this system model and show how to convert the OED problem in a dynamic physical network to one in a static logical graph which can be used to solve the OED problem in the dynamic physical network. We then propose a polynomial time greedy algorithm for computing satellite-assisted multi-hop entanglement paths. We also design an integer linear programming (ILP)-based algorithm to compute optimal solutions as a baseline to study the performance of our greedy algorithm. We present evaluation results to demonstrate the advantage of our model and algorithms.

1. INTRODUCTION

Predicated entirely on entanglement, quantum networks enable Alice to securely send information to Bob by teleporting the state of a qubit from her site to that of Bob without physically transferring the qubit itself, consuming the entanglement in the process. Entanglement is thus regarded as a precious resource in quantum communications, a currency dubbed *ebits*. The book by Van Meter [13] is considered an authoritative text on quantum networks, while Khatri and Wilde [6] provide a thorough mathematical treatment of quantum communications.

Repeaters in a quantum network employ local operations and classical communication (LOCC) to manipulate the state of one or more qubits in order to facilitate end-to-end entanglement between two parties who may not be directly connected by a physical communication link. We first generate entanglements between adjacent repeaters along links to form a repeater chain of entangled photon pairs between Alice and Bob. We then perform entanglement swapping [2] by applying a Bell state measurement (BSM) at each of the intermediate repeaters, transforming two consecutive entanglements into one, until Alice and Bob directly share an entangled photon

pair. Alice and Bob may now use this ebit to perform quantum teleportation. The entire process is assisted by classical heralding signals which indicate whether an attempt at entanglement generation or entanglement swapping is successful.

Through a strictly terrestrial lens, entanglement distribution on a global scale will always be hindered by photon loss over optical fibers, whose entanglement distribution rate decays exponentially with distance and is upper bounded by the repeaterless bound [10]. Satellites, particularly Low Earth Orbit (LEO) satellites, offer a promising workaround, as their low altitude makes entanglement distribution demonstrably achievable and their ability to travel in a periodic manner reduces the number of ground repeaters required to generate entanglement between two remote parties. A comprehensive review of the state-of-the-art work in space quantum communications can be found in [3, 12]. Entanglement distribution in a space-ground scheme can be accomplished in different ways, which we describe in the following.

The scheme proposed in [1] describes a *double downlink configuration*, in which satellites armed with entanglement sources beam down entangled photon pairs to two ground repeater stations at a time. Each ground repeater houses a number of quantum non-demolition (QND) measurement devices and quantum memories (QMs). If a satellite successfully transmits an entangled photon pair to two ground repeaters, with each repeater in possession of one photon, the successful attempt is heralded by the repeaters' QND devices. The repeaters then store the photons in their respective QMs until they receive information about successful entanglement distribution at neighboring repeaters, at which point they may perform BSMS to extend entanglements as needed.

The more recent architecture studied in [4, 7] allows for both ground and space repeaters. Satellites are not only fitted with entanglement sources, but also QND devices and QMs, so entanglement swapping can be executed in space as well as on Earth. Likewise, in addition to QND devices and QMs, ground stations may also be equipped with entanglement sources, so ground stations can distribute entanglement to satellites. In addition to *downlink channels*, these modifications allow for *uplink channels* and *inter-satellite links* [12].

Note that none of the aforementioned configurations require ground stations to directly transmit ebits to each other, which spares us the burden of mitigating photon loss over optical fibers. Our objective is to distribute ebits to a pair of ground stations purely by way of LEO satellites. This approach allows us to avoid optical fibers entirely in favor of free-space optical links in vacuum and only two atmospheric channels. The

Alena Chang, Yinxin Wan, Guoliang Xue, and Arunabha Sen are all affiliated with School of Computing and Augmented Intelligence, Arizona State University, Tempe, AZ 85287. Emails: {ahchang, ywan28, xue, asen}@asu.edu. Alena Chang and Yinxin Wan made equal contributions to this paper. This paper was supported in part by NSF grants 2007083 and 2007469. The information reported herein does not reflect the position of the policy of the funding agency.

entanglement distribution problem we study is in the vein of [9, 11], but we shift our attention to the celestial so as to align ourselves with the most probable future direction in quantum communications [3, 12].

Existing studies on satellite-based entanglement distribution from a networking standpoint often do not consider satellite movement over time and/or do not permit entanglement distribution along inter-satellite links. A satellite may be within communication range of a ground station or another satellite for them to share an entangled photon pair at one point in time, but they may be too far away from each other at a different point in time. A system model studying LEO satellite-based entanglement distribution should factor in the limitations on feasible photon transmission imposed by satellite movement. However, this has not been well investigated from a networking perspective.

LEO satellite-based entanglement distribution which excludes inter-satellite links poses a major hindrance due to the fact that the communication range of a single LEO satellite, given its low altitude, cannot accommodate two ground stations whose distance exceeds the communication range. If a ground station in New York City (NYC) and a ground station in Singapore request an ebit, a single LEO satellite cannot honor their request.

Prior networking papers on satellite-based entanglement distribution include [5, 8, 15]. The system model defined in [5] lays fundamental groundwork for modeling satellite-based entanglement distribution, taking into account satellite movement over time. However, the model only considers downlinks and does not permit inter-satellite links. Similarly, [8] only considers the double downlink configuration and also does not account for satellite movement. While [15] enables inter-satellite links and considers satellite movement, it focuses on a specific scenario consisting of three satellites connecting two ground stations, in which the central satellite is positioned halfway between the ground stations.

To the best of our knowledge, we are the first to investigate satellite-based entanglement distribution from a networking perspective at scale while taking into account satellite movement over time and inter-satellite links. The contributions of this paper are fourfold:

- We propose a system model of an LEO satellite-based quantum network which factors in both satellite movement over time and inter-satellite links, under which we define the optimal entanglement distribution (OED) problem.
- We introduce the concept of logical graphs and demonstrate how to construct the *static* logical graph corresponding to a set of connection requests in a *dynamic* physical network.
- We design a polynomial time greedy algorithm for solving the OED problem.
- We conduct extensive performance evaluation to demonstrate the advantage of our model and algorithms.

The remainder of this paper is organized as follows. In Section 2, we define the system model and the OED problem. In Section 3, we describe the concept of logical graphs as a means to solve the OED problem. In Section 4, we present

our algorithms for the OED problem. In Section 5, we present evaluation results together with our observations and analysis. Section 6 concludes the paper.

2. SYSTEM MODEL

In this section, we present the system model for the space-ground integrated quantum network. We also formulate the entanglement distribution problem to be studied.

A. Ground Stations and Moving Satellites

There are R equally spaced rings of satellites, and each ring passes over the North and South Poles in an arrangement known as a polar orbit. Each ring contains K evenly spaced satellites. The satellites are arranged so that they do not collide at the Poles. This kind of satellite constellation is known as a Walker Star constellation [14] and has been adopted in space-based entanglement distribution work such as [5]. Different from existing models [8, 15], we offer an at-scale model taking into consideration the movement of satellites. Consequently, the geolocation of a satellite dynamically changes and is determined by time, denoted by τ , where $\tau = 0$ means midnight, $\tau = 1$ means 1:00AM, etc. In contrast, the geolocation of a ground station is considered stationary. Fig. 1 illustrates an example of the type of network we study, with $R = 6$ and $K = 8$. In the figure, 28 satellites and 6 ground stations are visible, while there are a total of 48 satellites.

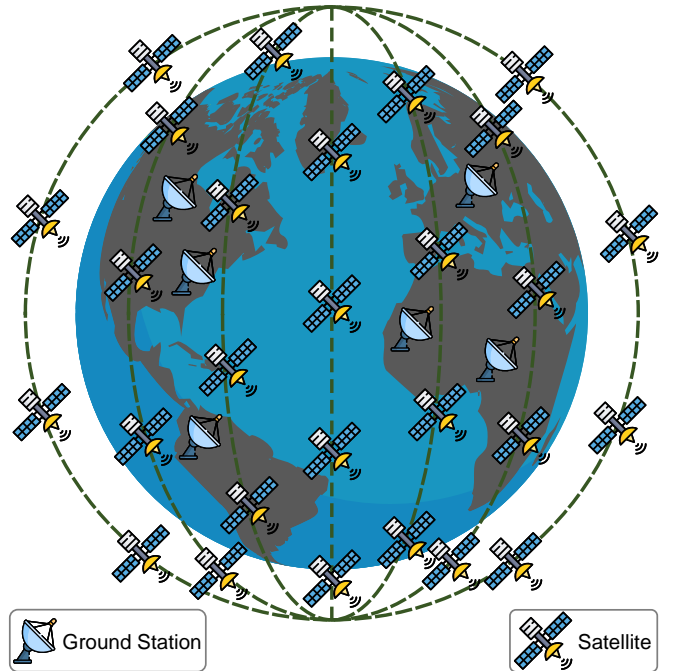


Fig. 1. An example of the type of network we study with $R = 6$ and $K = 8$.

Equipped with transmitters, receivers, and QMs, a satellite and another satellite or a ground station can establish a link if they are within each other's communication range. This distinguishes our model from existing models [5, 8] in that we allow inter-satellite links.

B. Problem Formulation

A connection request r_i is specified by a 4-tuple (s_i, t_i, d_i, w_i) , where s_i is the *source* node which corresponds to a ground

Section 4-B, we present an integer linear programming (ILP)-based approach for computing an optimal solution to OED . In Section 4-C, we discuss a variant of the ILP that can be used to compute optimal entanglement distribution without using inter-satellite links.

A. Polynomial Time Greedy Algorithm

Our greedy algorithm is presented in Algorithm 1. It considers the requests in non-increasing order of the reward-demand ratio. Whenever a request can be served, network resources are reserved for the corresponding connection request.

Algorithm 1: OED-Greedy

Input: Network state information and a set of connection requests \mathcal{R}

Output: A feasible subset $\mathcal{R}_{\text{greedy}}$ of \mathcal{R} and the service path π_i for each $r_i \in \mathcal{R}_{\text{greedy}}$

- 1 Sort the requests in \mathcal{R} in non-decreasing order of $\frac{w_i}{d_i}$. WLOG, assume that $\frac{w_1}{d_1} \geq \frac{w_2}{d_2} \geq \dots \geq \frac{w_N}{d_N}$.
- 2 Construct the logical graph $G(V, E)$ from the physical network and the set of connection requests \mathcal{R} .
- 3 $\mathcal{R}_{\text{greedy}} \leftarrow \emptyset$.
- 4 **for** $i := 1$ **to** N **do**
- 5 Compute a $l(s_i)$ - $l(t_i)$ path π_i of bandwidth at least d_i in G . Set $\pi_i \leftarrow \text{NULL}$ if such a path does not exist.
- 6 **if** $\pi_i \neq \text{NULL}$ **then**
- 7 Add r_i to $\mathcal{R}_{\text{greedy}}$.
- 8 Reserve the resources needed for path π_i .
- 9 Update graph G to its residual graph by removing the resources needed for path π_i .
- 10 **Output** $\mathcal{R}_{\text{greedy}}$ and $\{\pi_i | r_i \in \mathcal{R}_{\text{greedy}}\}$.

Algorithm 1 has a worst-case time complexity bounded by a lower-order polynomial. After sorting, the main steps of the algorithm consist of N path finding processes, each of which can be accomplished via breadth-first-search. While this algorithm does not guarantee to find an optimal solution, it is very fast, and can find close to optimal solutions in most cases, as demonstrated in our evaluations.

B. ILP-based Optimal Algorithm

In order to evaluate the performance of Algorithm 1, we design an Integer Linear Programming (ILP)-based algorithm. The main idea of our ILP-based algorithm is based on integer multi-commodity flows. For each request $r_i \in \mathcal{R}$, we associate a binary variable x_i . Here x_i is 1 if r_i is served, and 0 otherwise. For each edge $(u, v) \in E$, we associate N pairs of binary variables $f_i(u, v)$, $f_i(v, u)$, $i = 1, 2, \dots, N$. Here $f_i(u, v)$ is the amount of type- i flow from u to v . The ILP maximizes its linear objective function $\sum_{i=1}^N w_i \times x_i$, subject to linear constraints described as follows. *Flow out of a source node:* For each $i \in \{1, 2, \dots, N\}$, the net flow of type- i out of vertex $l(s_i)$ is x_i . *Flow into a destination node:* For each $i \in \{1, 2, \dots, N\}$, the net flow of type- i into vertex $l(t_i)$ is x_i . *Flow conservation:* For each $i \in \{1, 2, \dots, N\}$, for each vertex $z \in V$ that does not correspond to s_i or

t_i , i.e., $z \neq l(s_i)$ and $z \neq l(t_i)$, the net flow of type- i into vertex z is 0. *Channel capacity:* For each edge $(u, v) \in E$, $\sum_{i=1}^N (f_i(u, v) \times d_i + f_i(v, u) \times d_i)$ does not exceed the number of available channels between nodes $p(u)$ and $p(v)$. *Transmitters/Receivers/QMs:* If $f_i(u, v) = 1$, we need to reserve d_i transmitters at node $p(u)$, d_i receivers at node $p(v)$, and d_i QMs at both $p(u)$ and $p(v)$.

After solving the ILP described above, we can obtain an optimal solution to the OED problem. The optimal set of requests to be served is given by $\mathcal{R}_{\text{opt}} = \{r_i \in \mathcal{R} | x_i = 1\}$. The path π_i for $r_i \in \mathcal{R}_{\text{opt}}$ can be obtained by tracing out the edges (u, v) where $f_i(u, v)$ is 1.

C. Restricted ILP for Systems without Inter-satellite Links

To study the impact of allowing inter-satellite links in path computation, we also design a restricted ILP-based algorithm. The restricted ILP is a slight modification of the ILP studied in Section 4-B. The only modification is not allowing inter-satellite links.

5. PERFORMANCE EVALUATION

In this section, we present the evaluation results of our space-ground integrated quantum network model as well as our proposed algorithms. The evaluation was done on a workstation running Ubuntu 22.04 system with i9-12900 CPU and 64GB memory. ILP instances were solved using the Gurobi optimizer.

A. Evaluation Settings

Physical Network: We use 60 ground stations, each located in a major city in the world. Each physical network used in our evaluation consists of these 60 ground stations and $R \times K$ satellites, with $R = K$ taking a value in the set $\{1, 2, \dots, 25\}$. We set R and K to be the same so that the satellites are evenly distributed around the Earth. We set the altitude of the satellites as 550km and the orbital period as 1.5 hours, both of which are consistent with LEO satellites such as Micius from the QUESS (Quantum Experiments at Space Scale) project [3, 12]. In our evaluation, we use the line-of-sight to determine the communication range. As a result, the inter-satellite communication range is 4988.11km, and the communication range between a satellite and a ground station is 2703.81km. We assume the number of transmitters, receivers, and QMs at a node to be 10. The number of available channels between two nodes within their communication range is an integer between 1 and 5.

Connection Requests: The source and destination nodes comprising each connection request are chosen from the pool of 60 ground stations. The demand and reward for each connection request are integers between 1 and 5. We used $N = 1, 10, 20$, and 30 in our evaluations. Start time τ takes a value in the set $\{0.0, 0.5, 1.0, 1.5, \dots, 23.5\}$. We will describe the choice of δ in Section 5-B.

B. Evaluation Scenarios

We evaluate our model and algorithms in the following three scenarios:

- (i) In this scenario, \mathcal{R} consists of one connection request, between NYC and Singapore. The demand is 1 and the reward is 1. The start time is midnight. We study two cases. In the first case, we hold $R = K$ at 10 and 20, respectively, and let δ vary from 0.00 to 0.30 in increments of 0.01. In the second case, we hold δ at 0 and 0.1, respectively, and let $R = K$ vary from 1 to 25 in increments of 1. This scenario is designed to study the impact of allowing inter-satellite links on connecting two remote ground stations. In the first case, we study the impact of δ (for fixed R and K). In the second case, we study the impact of R and K (for fixed δ).
- (ii) In this scenario, \mathcal{R} consists of 20 connection requests, with the source and destination randomly chosen from the pool of 60 ground stations. The demand and reward for each request are random integers between 1 and 5. The start time is midnight for all 20 connection requests. We study two cases. In the first case, we hold $R = K$ at 10 and 20, respectively, and allow δ to vary from 0.00 to 0.30 in increments of 0.01. In the second case, we hold δ at 0.01 and 0.1, respectively, and let $R = K$ vary from 1 to 20 in increments of 1. This scenario is designed to study the impact of δ (for fixed R and K) and the impact of R and K (for fixed δ), in terms of total reward.
- (iii) In this scenario, for each value of $N = 10, 20$, and 30, we generate 48 different sets of connection requests: $\mathcal{R}_1^N, \mathcal{R}_2^N, \dots, \mathcal{R}_{48}^N$. Each \mathcal{R}_j^N consists of N connection requests where the source and destination are randomly chosen from the 60 ground stations, and the demand and reward are random integers between 1 and 5. All connection requests in \mathcal{R}_j^N have start time $0.5 \times (j - 1)$. For each of $R = K = 10, 15$, and 20, we evaluate the algorithms for each of $\delta = 0.1, 0.05, 0.01$, and 0.001. This scenario is designed to conduct a more extensive performance evaluation of the proposed algorithms, with the start times evenly distributed throughout the day.

C. Evaluation Results

In this section, we present evaluation results, together with our observations and analysis. We use *Greedy*, *ILP*, and *rILP* to denote the greedy algorithm, the ILP-based algorithm, and the restricted ILP-based algorithm, respectively.

Scenario (i): Fig. 3 illustrates the results of Scenario (i). Fig. 3(a) shows that *Greedy* (and *ILP*) can find a NYC-Singapore path for $\delta \leq 0.07$ when $R = K = 10$, and for $\delta \leq 0.15$ when $R = K = 20$. In contrast, *rILP* cannot find such a path for any $\delta = 0.00, 0.01, \dots, 0.30$ when both $R = K = 10$ and $R = K = 20$. This is because no single satellite can have a communication link with NYC and a communication link with Singapore at the same time.

Fig. 3(b) shows the result when we vary the value of $R = K$, with δ fixed. For $\delta = 0$, when $R = K \leq 6$, none of the algorithms can find a NYC-Singapore path. When $R = K \geq$

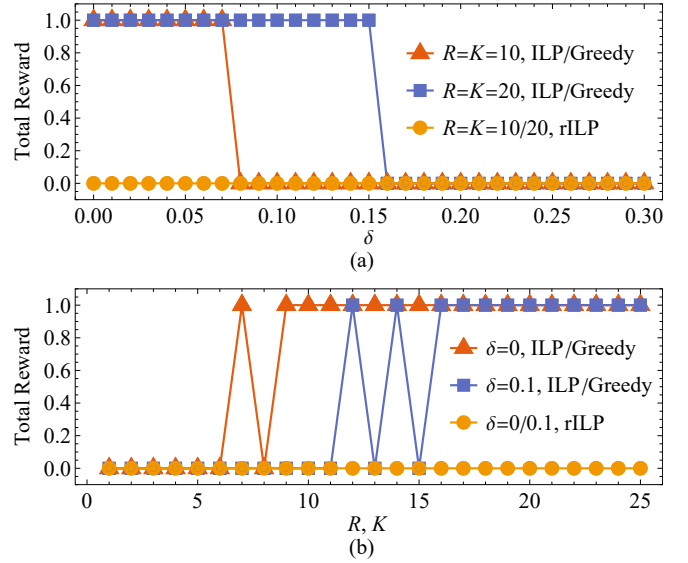


Fig. 3. Evaluation results of *Greedy*, *ILP*, and *rILP* with varying R , K , and δ for a single NYC-Singapore request with demand 1 and reward 1.

9, both *Greedy* and *ILP* can find a NYC-Singapore path. For $\delta = 0.1$, when $R = K \leq 11$, none of the algorithms can find a NYC-Singapore path. When $R = K \geq 16$, both *Greedy* and *ILP* can find a NYC-Singapore path.

Intuitively, when R and K increase, the number of edges in the logical graph also increases. But this is not always true. Hence we see the fluctuations in the figure. For $\delta = 0$, *ILP* has a reward value of 1 with $R = K = 7$, but the reward value drops to 0 when $R = K = 8$. An interesting observation is that, for a fixed time interval $[\tau, \tau + \delta]$, the total reward corresponding to *ILP* is non-decreasing when R (and K) is increased to $n \times R$ (and $m \times K$) for any integers $n \geq 1$ and $m \geq 1$. This is because the resulting logical graph is a super-graph of the original logical graph when R (and K) is increased to $n \times R$ (and $m \times K$). For $\delta = 0$, *ILP* has a reward value of 1 with $R = K = 7$. When R and K are increased to 14 (a multiple of 7), the reward does not decrease.

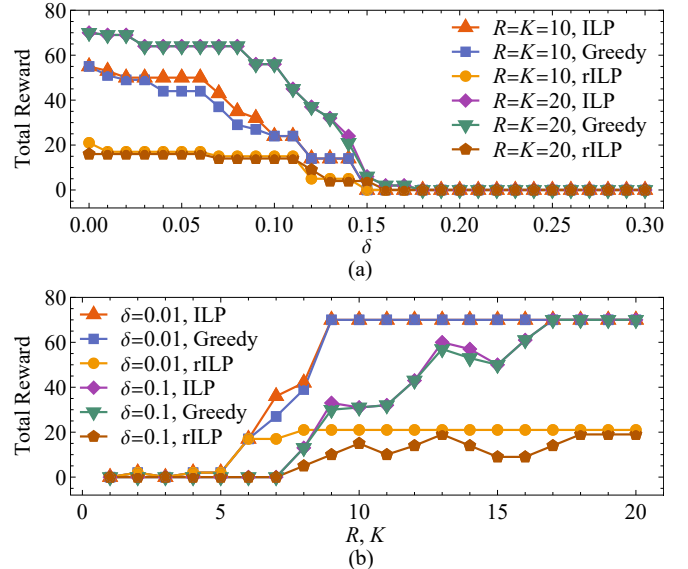


Fig. 4. Evaluations results of *Greedy*, *ILP*, and *rILP* with varying R , K , and δ for 20 randomly generated requests.

Scenario (ii): Fig. 4 illustrates the results of Scenario (ii). Fig. 4(a) shows the impact of δ on the total reward for each algorithm, with everything else fixed. We observe that the total reward is non-decreasing as δ increases. This is because fewer links will remain operational in the time interval $[\tau, \tau + \delta]$ when δ increases.

Fig. 4(b) shows the impact of R (and K) on the total reward for each algorithm, with δ fixed. We observe that the total reward is non-decreasing (with some fluctuations) as δ increases. As explained in Scenario (i), the total reward will be non-decreasing when R (and K) is increased to a multiple of R (and K). Therefore, fluctuations are possible.

Scenario (iii): Table 1 presents more extensive evaluation results. Unlike Scenarios (i) and (ii), we have connection requests with start time τ taking the values $0.5 \times (j - 1)$ for $j = 1, 2, \dots, 48$. This means we have starting times at every hour and every half hour.

Since the test cases have different time intervals, it is less meaningful to compute the total reward across all test cases. Rather, for each test case, we compute the ratio of the reward for Greedy over that for ILP, as well as the ratio of the reward for rILP over that for ILP, and take the average of these ratios. We also record the average running times for Greedy and ILP (the running time for rILP is similar to that for ILP). We observe that Greedy requires much less time than ILP, while computing solutions nearly as good as those computed by ILP.

TABLE 1
PERFORMANCE OF GREEDY, ILP, AND rILP FOR 1728 TEST CASES.

N	R, K	δ	rILP Ratio	Greedy Ratio	Greedy Time	ILP Time
10	10	0.1	0.1199	0.9966	0.0005s	0.1462s
		0.05	0.1359	0.9831	0.0006s	0.1600s
		0.01	0.1749	0.9982	0.0006s	0.1733s
		0.001	0.1809	0.9990	0.0006s	0.1789s
	15	0.1	0.0915	0.9860	0.0018s	0.6498s
		0.05	0.1803	1.0000	0.0021s	0.7640s
		0.01	0.2210	1.0000	0.0024s	0.8754s
		0.001	0.2272	1.0000	0.0024s	0.8875s
	20	0.1	0.1059	1.0000	0.0077s	3.5907s
		0.05	0.1945	1.0000	0.0089s	4.2291s
		0.01	0.2222	1.0000	0.0098s	4.7088s
		0.001	0.2287	1.0000	0.0101s	4.9035s
20	10	0.1	0.1393	0.9756	0.0009s	0.3519s
		0.05	0.1329	0.9643	0.0011s	0.3185s
		0.01	0.1606	0.9932	0.0012s	0.3430s
		0.001	0.1700	0.9936	0.0012s	0.3519s
	15	0.1	0.0868	0.9683	0.0034s	1.3464s
		0.05	0.1576	1.0000	0.0038s	1.5269s
		0.01	0.1980	1.0000	0.0043s	1.7278s
		0.001	0.2056	1.0000	0.0044s	1.7764s
	20	0.1	0.0959	1.0000	0.0146s	6.9379s
		0.05	0.1719	1.0000	0.0168s	8.1285s
		0.01	0.2074	1.0000	0.0186s	9.0636s
		0.001	0.2128	1.0000	0.0191s	9.2650s
30	10	0.1	0.1618	0.9523	0.0014s	0.4592s
		0.05	0.1296	0.9311	0.0017s	0.5930s
		0.01	0.1517	0.9685	0.0018s	0.6046s
		0.001	0.1569	0.9736	0.0018s	0.6210s
	15	0.1	0.0834	0.9455	0.0055s	2.3433s
		0.05	0.1441	0.9978	0.0074s	2.9550s
		0.01	0.1856	1.0000	0.0084s	3.4108s
		0.001	0.1945	1.0000	0.0086s	3.4192s
	20	0.1	0.0965	0.9981	0.0215s	10.6800s
		0.05	0.1649	1.0000	0.0247s	14.7769s
		0.01	0.1929	1.0000	0.0274s	16.4577s
		0.001	0.1992	1.0000	0.0281s	16.9239s

6. CONCLUSIONS

In this paper, we have proposed a system model for a space-ground integrated quantum network. Unlike previous research, we take into consideration the movement of the satellites and inter-satellite links. We also ensure that all links used in the computed entanglement paths are guaranteed to be operational within an entire time interval.

To study entanglement distribution in such a dynamic network, we propose a novel concept of logical graphs. We design a polynomial time greedy algorithm for solving the entanglement distribution problem in a dynamic physical network with the aid of the corresponding logical graph.

We demonstrate that it is possible to establish an NYC-Singapore path using inter-satellite links. Extensive evaluations show that our greedy algorithm can compute solutions that are nearly as good as optimal, while using much less time.

REFERENCES

- [1] K. Boone, J.-P. Bourgoin, E. Meyer-Scott, K. Heshami, T. Jennewein, and C. Simon, "Entanglement over global distances via quantum repeaters with satellite links," *Phys. Rev. A*, vol. 91, no. 5, 2015.
- [2] A. Chang and G. Xue, "Order matters: On the impact of swapping order on an entanglement path in a quantum network," in *Proc. of IEEE INFOCOM WKSHPs*, 2022.
- [3] L. d. F. de Parny, O. Alibert, J. Debaud, S. Gressani, A. Lagarrigue, A. Martin, A. Metrat, M. Schiavon, T. Troisi, E. Diamanti, P. Gélard, E. Kerstel, S. Tanzilli, and M. V. D. Bossche, "Satellite-based quantum information networks: use cases, architecture, and roadmap," *Commun. Phys.*, vol. 6, no. 12, 2023.
- [4] M. Gündoğan, J. S. Sidhu, V. Henderson, L. Mazzarella, J. Wolters, D. K. L. Oi, and M. Krutzik, "Proposal for space-borne quantum memories for global quantum networking," *npj Quantum Information*, vol. 7, no. 128, 2021.
- [5] S. Khatri, A. J. Brady, R. A. Desporte, M. P. Bart, and J. P. Dowling, "Spooky action at a global distance: analysis of space-based entanglement distribution for the quantum internet," *npj Quantum Information*, vol. 7, no. 4, 2021.
- [6] S. Khatri and M. M. Wilde, "Principles of quantum communication theory: A modern approach," *arXiv preprint arXiv:2011.04672*, 2020.
- [7] C. Liorni, H. Kampermann, and D. Bruß, "Quantum repeaters in space," *New Journal of Physics*, vol. 23, no. 5, 2021.
- [8] N. K. Panigrahy, P. Dhara, D. Towsley, S. Guha, and L. Tassiulas, "Optimal entanglement distribution using satellite based quantum networks," in *Proc. of IEEE INFOCOM WKSHPs*, 2022.
- [9] M. Pant, H. Krovi, D. Towsley, L. Tassiulas, L. Jiang, P. Basu, D. Englund, and S. Guha, "Routing entanglement in the quantum internet," *npj Quantum Information*, vol. 5, no. 25, 2019.
- [10] S. Pirandola, R. Laurenza, C. Ottaviani, and L. Banchi, "Fundamental limits of repeaterless quantum commu-

- nications,” *Nature Communications*, vol. 8, no. 15043, 2017.
- [11] S. Shi and C. Qian, “Concurrent entanglement routing for quantum networks: Model and designs,” in *Proc. of ACM SIGCOMM*, 2020.
- [12] J. S. Sidhu, S. K. Joshi, M. Gündoğan, T. Brougham, D. Lowndes, L. Mazzarella, M. Krutzik, S. Mohapatra, D. Dequal, G. Vallone, P. Villorosi, A. Ling, T. Jennewein, M. Mohageg, J. G. Rarity, I. Fuentes, S. Pirandola, and D. K. L. Oi, “Advances in space quantum communications,” *IET Quantum Communication*, vol. 2, no. 4, pp. 182–217, 2021.
- [13] R. Van Meter, *Quantum Networking*. John Wiley & Sons, 2014.
- [14] J. G. Walker, “Circular orbit patterns providing continuous whole earth coverage,” Royal Aircraft Establishment, Tech. Rep., 1970.
- [15] J. Wallnöfer, F. Hahn, M. Gündoğan, J. S. Sidhu, F. Wiesner, N. Walk, J. Eisert, and J. Wolters, “Simulating quantum repeater strategies for multiple satellites,” *Communications Physics*, vol. 5, no. 169, 2022.